Electronic Supplementary Material (ESI) for Nanoscale.


*Electronic Supplementary Information*

# Synthesis of Multiphase $MoS_2$ Heterostructures using Temperature-controlled Plasma-sulfurization for Photodetector Applications

*Kubra Aydin[a,b,†], Chaitanya Kanade[a,b,c,†], Vinit Kaluram Kanade[a,b], Gulgun Bahit[d], Chisung Ahn[e,*] and Taesung Kim[a,b,d,f,*]*

Dr. C. Ahn

E-mail: cahn@kitech.re.kr

Prof. T. Kim

E-mail: tkim@skku.edu

[*] Authors to whom correspondence should be addressed

**Table S1** Synthesis conditions for 1T- and 2H-$MoS_2$.

| **$MoS_2$ Phase** | **Method** | **Substrate** | **Gas** | **Flow Rate [sccm]** | **Temperature [°C]** | **Process Time [h]** |
|---|---|---|---|---|---|---|
| 1T-$MoS_2$ | PECVD | Si | Ar:$H_2$ | 10:10 | 150 | 1.5 |
| 2H-$MoS_2$ | PECVD | Si | Ar:$H_2$ | 10:10 | 300 | 1.5 |

X-ray photoelectron spectroscopy (XPS) analyses were performed on the 1T/1T- and 2H/2H-$MoS_2$ monostructures and 2H/1T-$MoS_2$ heterostructures, as shown in Figure S1. In Figure S1a, the peaks at approximately 229.2 and 232.6 eV correspond to the $3d_{5/2}$ and $3d_{3/2}$ peaks of $Mo^{4+}$, respectively, corresponding to 2H-$MoS_2$.[1] The 1T-$MoS_2$ peaks were located at a lower energy of approximately 0.7 eV.[2] In Figure S1b, the S $2p_{3/2}$ and S $2p_{1/2}$ peaks were observed at 161.4 and 162.8 eV for the 1T phase, whereas the binding energies corresponding to 2H-$MoS_2$ were observed at 162.2 and 163.7 eV.[3] In Figures S1c and S1d, all the peaks formed in 2H/2H-$MoS_2$ corresponded to the 2H phase. In the XPS graphs of 2H/1T-$MoS_2$ (Figures S1e and S1f for Mo 3d and S2p, respectively), the 2H and 1T phase peaks were located together, indicating that both phases were formed in the 2H/1T structure.

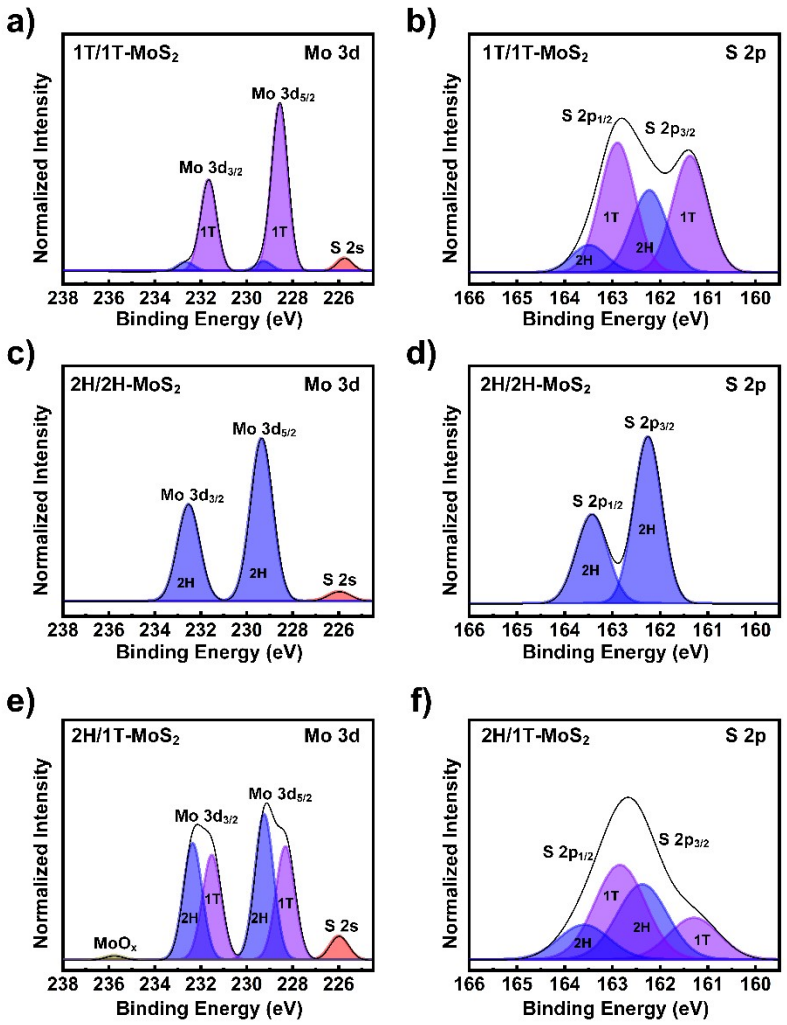


**Figure S1.** XPS surface analysis for (a) Mo 3d and (b) S 2p of 1T/1T-$MoS_2$; (c) Mo 3d and (d) S 2p of 2H/2H-$MoS_2$; and (e) Mo 3d and (f) S 2p of 2H/1T-$MoS_2$.

XPS depth profile analyses were performed to determine the elemental distribution from the surface to the interior of the 2H/1T-$MoS_2$ heterostructure. A high-energy Ar ion beam was used to etch the samples layer-by-layer at 120 s intervals for each etching cycle. An elemental distribution change from the 2H phase-related peak to the 1T phase-related peak in the XPS profiles from the surface to the lower layers was observed in the Mo 3d core peak profiles until the 4$^{th}$ cycle. In contrast, the peak initially formed at the S 2p core peak owing to the 2H phase decreased and broadened in the 2$^{nd}$ cycle and then disappeared in the 4$^{th}$ cycle. This decrease and broadening of the peak are due to the damage it causes to the Ar-ion beam S.[4]

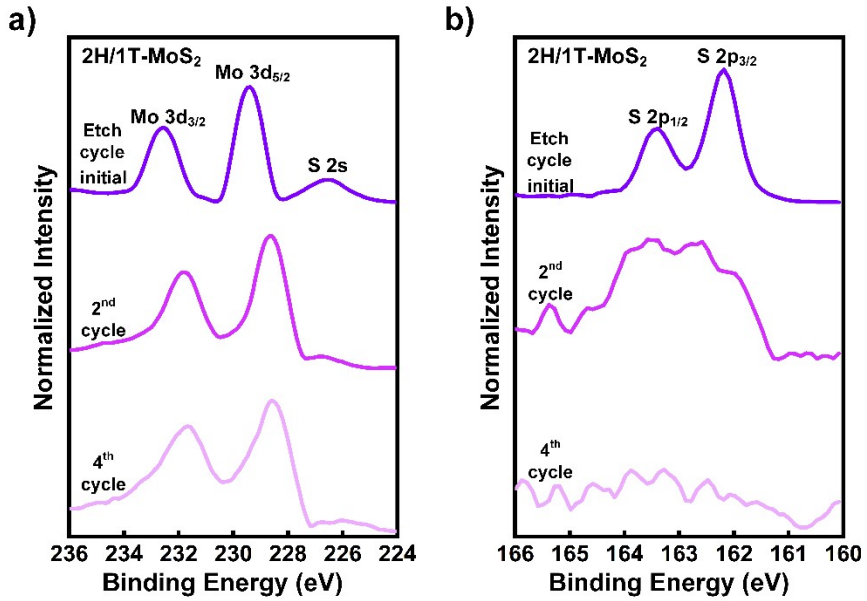


**Figure S2.** 2H/1T-$MoS_2$ XPS depth profiling analysis for (a) the Mo 3d and (b) S 2p core peak levels.

The enlarged HRTEM images in Figures S3a and S3b show the trigonal lattice area of the 1T phase and common honeycomb lattice area of the 2H phase in 1T/1T- and 2H/2H-$MoS_2$, respectively.[5] Unlike these two heterostructures, the 2H/1T-$MoS_2$ heterostructure exhibited an edge-exposed HRTEM image similar to that of 1T/2H-$MoS_2$.

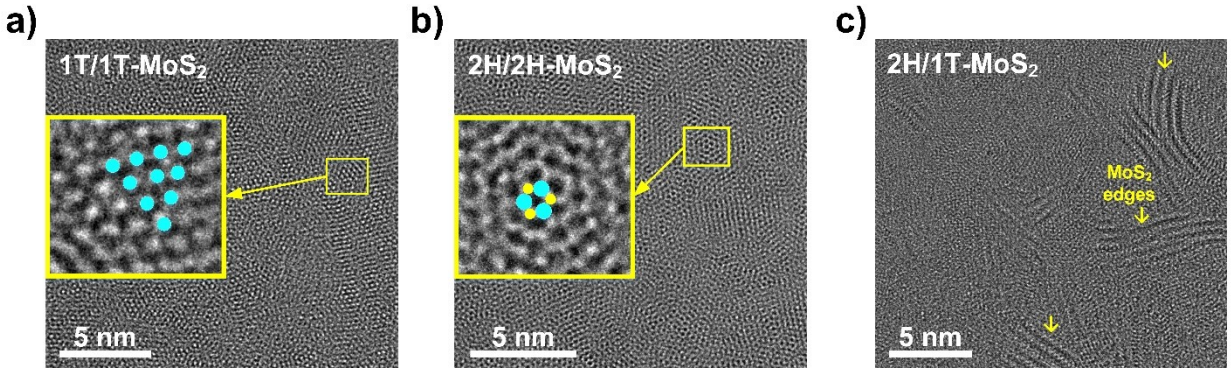


**Figure S3.** HRTEM top view images of (a) the 1T/1T- and (b) 2H/2H-$MoS_2$ monostructures, and (c) 2H/1T-$MoS_2$ heterostructures.

The photoresponsivity and detectivity values of 1T/1T-, 2H/2H-, and 2H/1T-$MoS_2$ are shown in Figure S4 under illumination at 420, 530, 660, and 1050 nm. Although the photocurrent was 634 nA for the 1T/1T-$MoS_2$ monostructure, an equal change of 430 nA was observed for the 2H/2H-$MoS_2$ monostructure and the 2H/1T-$MoS_2$ heterostructures under light irradiation.

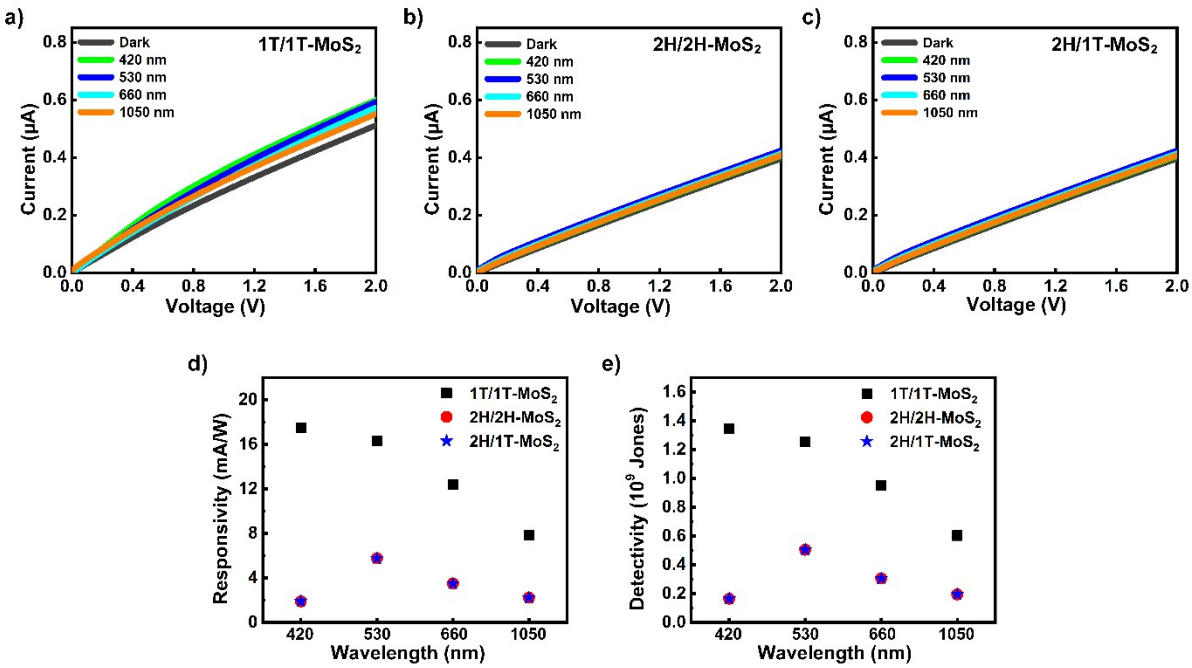


**Figure S4.** Current-voltage output curves of (a) 1T/1T-$MoS_2$, (b) 2H/2H-$MoS_2$, and (c) 2H/1T-$MoS_2$ on Si under various wavelength illuminations. (d) Photoresponsivity and (e) detectivity analysis of 1T/1T-, 2H/2H- and 2H/1T-$MoS_2$ under 5 μW of 420, 530, 660, and 1050 nm laser.

**Table S2.** Comparison of the photoresponsivity, detectivity, and rise ($\tau_r$) and decay ($\tau_D$) times for the 1T/2H-$MoS_2$ heterostructure with other materials in the literature.

| **Material** | **Synthesis Method** | **Wavelength (nm)** | **Responsivity (mA/W)** | **Detectivity (Jones)** | **Rise ($\tau_r$) and decay ($\tau_d$) times (ms)** | **Reference** |
|---|---|---|---|---|---|---|
| 1T/2H-$MoS_2$ | PECVD | 530 | 23.56 | $1.58 \times 10^9$ | 90, 30 | This study |
| $MoS_2$-$ReS_2$ | APCVD | 800 | $42.61 \times 10^3$ | $2.81 \times 10^{13}$ | 20, 19 | [6] |
| $MoS_2$/p-Si | CVD | 532 | $117 \times 10^3$ | $\sim 10^9$ | 84, 136 | [7] |
| $MoS_2$/β-$Ga_2O_3$ | Thermolysis | 245 | 2.05 | $1.21 \times 10^{11}$ | - | [8] |
| Ge-gated $MoS_2$ | Mechanical Exfoliation | 520 | $2.18 \times 10^3$ | - | 15 | [9] |

| | | | | | | |
|---|---|---|---|---|---|---|
| $MoS_2$-GQDs | CVD | 405 | $1.6 \times 10^7$ | - | 70, $12.2 \times 10^3$ | [10] |
| SL $MoS_2$ | Mechanical Exfoliation | 550 | 7.5 | - | 50 | [11] |

## Calculations for photomeasurement study:

For 1T/2H heterostructure under 530 nm light source of $P_{light}$ = 1 µW power used.

$I_{illumination} = 6.963 \times 10^{-07}$ A

$I_{dark} = 6.727 \times 10^{-07}$ A

$I_{photo} = I_{illumination} - I_{dark}$

$I_{photo} = 6.963 \times 10^{-07} - 6.727 \times 10^{-07}$

$I_{photo} = 2.356 \times 10^{-08}$ A

Responsivity calculated from using equation (1)

$R = I_{photo}/P_{light} = 2.356 \times 10^{-08}$ A/ $1 \times 10^{-06}$ W = $2.356 \times 10^{-02}$ A/W

Responsivity; R = 23.56 mA/W

The detectivity is calculated using equation (4)

$D^* = R(A)^{1/2} / (2.e.\ I_{dark})^{1/2}$

Where; R= $2.356 \times 10^{-02}$ A/W

Area between two electrodes due to light spread is bigger than the electrode area; Hence effective area is A = 95 µm × 1020 µm = 96900 $\mu m^2$ = $9.69 \times 10^{-4}$ $cm^2$

E= electron/elementary charge = $1.6021 \times 10^{-19}$ C

$I_{dark} = 6.727 \times 10^{-07}$ A

Detectivity; $D^* = R(A)^{1/2} / (2.e.\ I_{dark})^{1/2}$

$= 2.356 \times 10^{-02} \times (9.69 \times 10^{-4})^{1/2} / (2 \times 1.6021 \times 10^{-19} \times 6.727 \times 10^{-07})^{½}$

$= 1.58 \times 10^{09}$ cm·$Hz^{1/2}$/W

$= 1.58 \times 10^{09}$ Jones

**References:**


[1] H. Fan, R. Wu, H. Liu, X. Yang, Y. Sun, C. Chen, *J. Mater. Sci.*, 2018, **53**, 10302.

[2] G. Wang, G. Zhang, X. Ke, X. Chen, X. Chen, Y. Wang, G. Huang, J. Dong, S. Chu, M. Sui, *Small*, 2022, **18**, 2107238.

[3] X. Sun, Y. Pang, S. Li, Y. Yu, X. Ding, L. Wang, Q. Zhang, *Ceram. Int.*, 2022, **48**, 21358.

[4] S. Hussain, J. Singh, D. Vikraman, A. K. Singh, M. Z. Iqbal, M. F. Khan, P. Kumar, D.-C. Choi, W. Song, K.-S. An, J. Eom, W.-G. Lee, J. Jung, *Sci. Rep.*, 2016, **6**, 30791.

[5] L. Cai, J. He, Q. Liu, T. Yao, L. Chen, W. Yan, F. Hu, Y. Jiang, Y. Zhao, T. Hu, Z. Sun, S. Wei, *J. Am. Chem. Soc.*, 2015, **137**, 2622.

[6] R. Wadhwa, A. V. Agrawal, D. Kushavah, A. Mushtaq, S. K. Pal, M. Kumar, *Appl. Surf. Sci.*, 2021, **569**, 150949.

[7] X. Liu, F. Li, M. Xu, T. Shen, Z. Yang, W. Fan, J. Qi, *Langmuir*, 2018, **34**, 14151.

[8] R. Zhuo, D. Wu, Y. Wang, E. Wu, C. Jia, Z. Shi, T. Xu, Y. Tian, X. Li, *J. Mater. Chem. C*, 2018, **6**, 10982.

[9] S.-G. Kim, S.-H. Kim, J. Park, G.-S. Kim, J.-H. Park, K. C. Saraswat, J. Kim, H.-Y. Yu, *ACS Nano*, 2019, **13**, 10294.

[10] C. Chen, H. Qiao, S. Lin, C. M. Luk, Y. Liu, Z. Xu, J. Song, Y. Xue, D. Li, J. Yuan, W. Yu, C. Pan, S. P. Lau, Q. Bao, *Sci. Rep.*, 2015, **5**, 1.

[11] Z. Yin, H. Li, H. Li, L. Jiang, Y. Shi, Y. Sun, G. Lu, Q. Zhang, X. Chen, H. Zhang, *ACS Nano*, 2012, **6**, 74.